Journal of Sustainable Metallurgy (2022) 8:715–731
https://doi.org/10.1007/s40831-022-00520-0

RESEARCH ARTICLE

Recovery of Some Rare-Earth Elements by Sorption Technique onto Graphene Oxide

Ehab A. A. El-Shazly[1] · Saber I. Moussa[1] · Gehan A. Dakroury[1]

Received: 30 September 2021 / Accepted: 17 March 2022 / Published online: 19 April 2022

Abstract

In this work, graphene oxide (GO), prepared using the Hummers method, is physically characterized and used for rare-earth metals recovery from monazite ores. Batch study for sorption of $^{152+154}$Eu radionuclide onto GO carried out to assess the optimum reaction parameters for recovery process. The optimum pH is 2.09, the equilibrium time achieved after 5 h, humic acid enhances the sorption efficiency but if its concentration increases it opposes the sorption process. The kinetic reaction mechanism is regulated by pseudo-2nd order and the sorption isotherms show Langmuir applicability. The maximum sorption capacity for $^{152+154}$Eu at 20 °C is 59.81 mg g^{-1}. Desorption studies were performed to determine a proper eluent with a suitable concentration for the recovery process and 0.1 M HCl was selected as an efficient eluent. The sorption process is favorable and endothermic. Finally, GO is used as a sorbent for rare-earth elements accumulated in monazite ore. The sorption efficiency of REE is 69.03% with initial concentration 1149.57 mg L^{-1} at monazite leachate and the recovery percentage is 20.32%. These results promised the use of GO for REE recovery from monazite ore.

Graphical Abstract

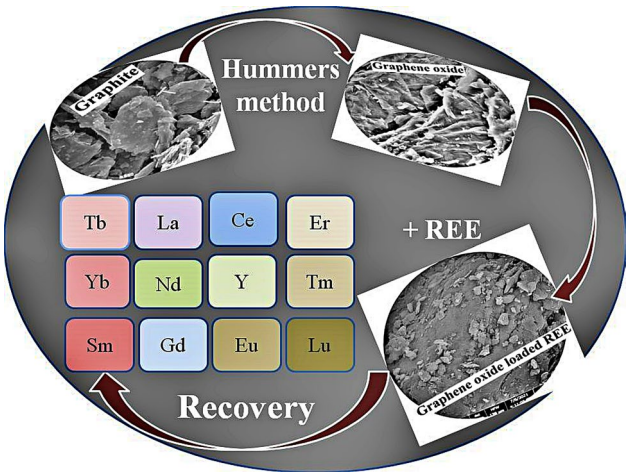

Keywords Adsorption · Graphene oxide · Radioactive Eu (III)

The contributing editor for this article was Atsushi Shibayama.

✉ Ehab A. A. El-Shazly
ehabelshazly2010@hotmail.com

[1] Nuclear Chemistry Department, Radioisotopes Production and Radiation Sources Division Hot Laboratories Centre, Egyptian Atomic Energy Authority, P.O. 13759, Cairo, Egypt

Introduction

Rare-earth elements, (REE), occur mostly in bastnaesite, monazite, together with xenotime ores, which represent about 95% of their occurrence in nature [1]. They can also be found in silicates, halides, carbonates, and phosphates but in low concentrations and in impure. Monazite ore is the

second most important ore in the world. Rare-earth elements (REE) have technical importance due to their wide application in different areas [2, 3], as these elements are named "The Vitamins of Modern Industry" [1]. They are used for electronic purposes, metallurgy, medical science, and optical technology. The demand for REE has grown rapidly over the years, more than its supply rate. Many techniques are used for the recovery of REE to overcome this problem, such as ion exchange [4], co-precipitation [5], membrane [6], solvent extraction [7], electrochemical [8], and adsorption [9]. Adsorption techniques are widely used due to their fast, easy operation and low cost. The efficiency of the adsorption process depends on the accessibility of the adsorbent.

Researchers pay significant attention to graphene oxide (GO) as it is an effective adsorbent for REE [10, 11]. The hexagonal structure of GO contains several function groups as hydroxyl, alkoxy, carbonyl), carboxylic acid, and other oxygen-based functional groups [12]. These oxygenated groups are responsible for many advantages, including higher solubility [13] and the possibility for surface functionalization [14]. This makes the GO a potential adsorbent. Limited studies have been reported on GO adsorption due their high cost. Graphene and related materials cannot be used in cheap, large-scale production, and lower electrical and thermal conductivity [15]. Here, the authors decided to use GO for bi-function as an adsorbent for $^{152+154}$Eu from radioactive waste and for recovery of rare-earth elements from low-grade monazite in Egypt.

This work aims to prepare graphene oxide from graphite by the Hummers method and use it for REE recovery from monazite leachate by the sorption technique. Physicochemical analytical techniques such as FTIR, DTA-TGA, SEM, XRD, and pore size analysis were carried out on the prepared GO. Optimization of the basic parameters such as pH, contact time, metal ion concentration, ionic strength, presence of humic acid (HA), and temperature affects the sorption reaction performed by examination the sorption behavior of $^{152+154}$Eu radionuclide onto the GO. A desorption study was also performed on the $^{152+154}$Eu radionuclide to determine the best eluent with the proper concentration to be used in REE recycling. The kinetics models and isotherm models were applied to identify the mechanism of the sorption reaction. The spontaneity of the process is clarified by thermodynamic study.

Experimental

Materials and Procedures

Reagents

Graphite (fine powder, extra pure) was purchased from Merck & Co., Germany. Potassium permanganate ($KMnO_4$) was purchased from BDH chemicals, Ltd., England. $NaNO_3$ and sulfuric acid (H_2SO_4, 95–97%) were purchased from Sigma-Aldrich. Hydrogen peroxide (H_2O_2, 30%, Alpha, India). Merck & Co., Germany supplied the sodium salt of humic acid. All chemicals used were of analytical grade purity and were used without further purification.

Eu_2O_3 salts got from Merck Co., Germany, and irradiated in the 2nd Egyptian Research Reactor (ET-RR-2) with a neutron flux of 10^{14} n cm^{-2} s^{-1} for 48 h at 22 MW to produce $^{152+154}$Eu radioisotopes. The irradiated target was left for a period to cool. After cooling, the irradiated Eu_2O_3 was dissolved in a certain volume of 1 M HCl which evaporated till dryness and re-dissolved in a double-distilled water. The initial activity of the selected radioisotope was 100 KBq L^{-1}. A stock solution of $^{152+154}$Eu radionuclide was prepared using a certain concentration of Eu (III) salts before spiking with the $^{152+154}$Eu radioisotope.

Monazite concentrate (monazite content of about 90%) is supplied by the nuclear materials authority in Cairo, Egypt. For pH adjustment, HCl and NaOH obtained from ADWIC (Egypt).

Sorbent Preparation

GO was prepared using pure natural graphite powder as a precursor according to the Hummers method [16]. This method gives numbers of layers in GO structure, reproducibility, and a great amount of oxygen [17]. In this method, 0.5 g of graphite mixed with 0.5 g of $NaNO_3$ followed by adding 23 mL of concentrated H_2SO_4 while vigorously stirring for nearly 3 h till a homogenous heavy gelatinous is obtained. Then, 3 g $KMnO_4$ was added gradually to the above liquid solution and the temperature must be kept below 20 °C. The mixture was stirred at room temperature (20 °C for 2 h), and therefore, the resulting solution was diluted by adding 30 mL of distilled water, and 10 mL of 30% H_2O_2 was added to the suspension to convert the remaining permanganate and manganese dioxide into soluble sulfate. The resulting mixture was washed several times with bi-distilled water and sonicated using ultrasonic apparatus for an hour, and the remaining solid material was dried at 80 °C for 24 h to obtain graphene oxide sheets.

Preparation of REEs Solutions

Monazite material is digested by caustic soda [18]. The digested REEs dissolved carefully in 50 mL concentrated HCl acid in a water bath at 85 °C. The initial concentration of REEs solutions is 1149.57 mg L^{-1}.

Instruments

The functional groups are identified by utilizing the Bomen Miclson FTIR spectrophotometer, model MB157, Canada. The amorphous and/or crystalline phase structure was clarified using Shimadzu X-ray diffraction (XRD), model XD-Dl, Kyoto, Japan, with a diffraction angle (2θ) range of 4°–70°. The thermal stability is measured by DTA-TGA-50, Japan, at a constant rate of 5 °C min^{-1} from room temperature to 650 °C. The particles morphology was investigated by JEOL JSM-5400, Japan. (SEM, FEI Quanta FEG-250, EDX) for SEM. Pore size distribution and corresponding porosity were calculated with the aid of pore-sizer chromatech 9320, USA. The activity of radionuclides has been determined radiometrically by high-resolution (7.5%) NaI (Tl) detector model 802-3X3, Canberra, (USA). An Inductive-Coupled Plasma Optical Emission Spectrometer (Prodig Axial high-dispersion ICP-OES model, USA) was used to measure the concentration of rare earth recovered from monazite by sorption and desorption.

Batch Study

The sorption behavior of **$^{152+154}$Eu** radionuclide achieved using a batch technique, by contacting 0.1 g of the GO with 10 mL of an initial concentration of (100–1000 mg L^{-1}) of Eu(III) labeled with $^{152+154}$Eu radioisotope at various time ranges (5–2880 min), temperatures (20 °C, 30 °C, 40 °C, and 50 °C), and the pH will be established according to the study of the effect of the pH 2.09.

The uptake percentage of radionuclides is measured and sorbed amount q (mg g^{-1}) is calculated using Eqs. (1) and (2), respectively. The distribution coefficient K_d (mL g^{-1}) given by Eq. (3):

$$\%\text{Uptake} = \left(\frac{A_o - A_e}{A_o}\right)100\%, \tag{1}$$

$$q = \frac{A_o - A_e}{A_o} C_0 \frac{V}{m}, \tag{2}$$

$$k_d = \left(\frac{A_o - A_e}{A_o}\right)\frac{V}{m}, \tag{3}$$

where A_o and A_e denote the activity of $^{152+154}$Eu radionuclide in aqueous solution before and after the sorption process, respectively. C_o denotes the initial concentration of Eu(III) in mg L^{-1}, V denotes the volume of aqueous solution (L for q and mL for K_d), and m denotes the weight of the graphene oxide (g).

Kinetic Modeling

The mechanism of the sorption reaction could be predicted by applying kinetic modeling at 20 °C. The non-linear pseudo-1st-order model [19], the non-linear pseudo-2nd-order model [20] and intraparticle diffusion model [21] Eqs. (4, 5, 6), respectively.

$$q_{t=}q_{e(cal.)}\left(1 - e^{-K_1 t}\right), \tag{4}$$

$$q_t = \frac{K_2 q_{e(cal.)}^2 t}{1 + K_2 q_e t}, \tag{5}$$

$$q_t = K_{id} t^{0.5} + C, \tag{6}$$

where the amounts of metal sorbed (mg g^{-1}) at equilibrium time and at any time (t) are represented by q_e and q_t, respectively. The pseudo-1st-order rate constant is denoted by k_1 (min^{-1}) while k_2 (g mg^{-1} min^{-1}) is the pseudo-2nd-order rate constant. The k_{id} (mg g^{-1} $min^{-0.5}$) is the intraparticle diffusion rate constant and the intercept given by C.

Isotherm Modeling

Three different isotherm models were checked to recognize the behavior of interaction of $^{152+154}$Eu radionuclide on graphene oxide at 20 °C; Langmuir [22], Freundlich [23], and the Dubinin–Radushkevich (D–R) model [24].

The non-linear relation of the Langmuir model can be expressed as Eq. (7):

$$q_e = \frac{q_m b C_e}{1 + bC_e}, \tag{7}$$

where q_m is the monolayer sorption capacity (mg g^{-1}), b is the free energy of sorption ($b\ \alpha\ e^{-\Delta G/RT}$), and C_e is the equilibrium metal ion concentration.

Using the Langmuir equilibrium parameter, the favorability of the isotherm can be recognized by applying Eq. (8) and determined the value of R_L [25].

$$R_L = \frac{1}{1 + bC_o}, \tag{8}$$

Co is that the initial metal ion concentration. The value of R_L is used as a sign for the isotherm linear ($R_L = 1$),

irreversible ($R_L = 0$), unfavorable ($R_L > 1$), or favorable ($0 < R_L < 1$).

Also, the non-linear form of the Freundlich model can be expressed in Eq. (9) as the following:

$$q_e = K_f C_e^{\frac{1}{n}}, \tag{9}$$

where K_f is the Freundlich sorption capacity coefficient (mg g^{-1}), and $1/n$ is that the adsorption intensity.

The (D–R) model is given by Eq. (10):

$$q_m = e^{-\beta\varepsilon^2}, \tag{10}$$

where q_m is monolayer capacity, β is a constant related to apparent adsorption energy $E = 1/(2\beta)^{1/2}$, and ε is polanyi potential and can be calculated from Eq. (11):

$$\varepsilon = \mathrm{RTln}\left(1 + \frac{1}{C_e}\right), \tag{11}$$

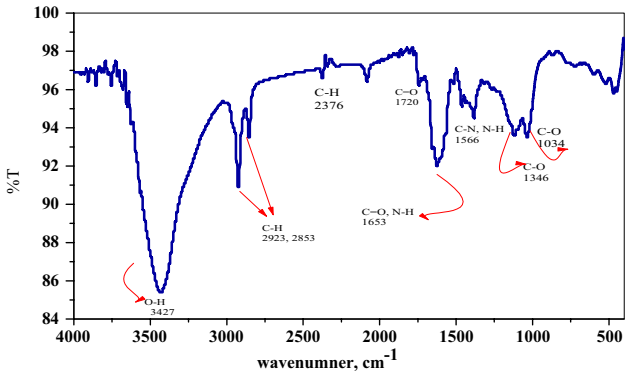

Fig. 1 FTIR of GO prepared by modified Hammer method at 20 °C

where R is the gas constant equal to 8.314 J K^{-1} mol^{-1} and T is the temperature degree (K).

Thermodynamic Study

The Gibbs free energy of sorption, ΔG (kJ mol^{-1}) is determined from Eq. (12–15):

$$\Delta G^o = \Delta H^o - T\Delta S^o \tag{12}$$

Applying Van't Hoff equation for corrected dimensionless equilibrium constant [26].

$$\Delta G^o = -\mathrm{RTln}\, K^o, \tag{13}$$

$$\ln K^o = 1000 \cdot K_g \cdot d, \tag{14}$$

$$K^O = 1000 \cdot K_g \cdot 55.51 \cdot \text{Molecular weight}, \tag{15}$$

where R denotes the universal gas constant 8.314 J mol^{-1} K^{-1}, and T is the absolute temperature. The molar concentration of water in an aqueous solution is 55.51 as 1 kg of water will occupy a volume of 1 L.

Desorption Studies

The desorption of $^{152+154}$Eu radionuclide was carried out by mixing the loaded GO with 10 mL of eluents in 50 mL glass bottles and shaken them at 180 rpm. The eluents $FeCl_3$, oxalic acid, EDTA, and HCl of various concentrations (0.01 mol L^{-1}, 0.05 mol L^{-1}, and 0.1 mol L^{-1}) were used. The recovery percentage (%) was determined using Eq. (16):

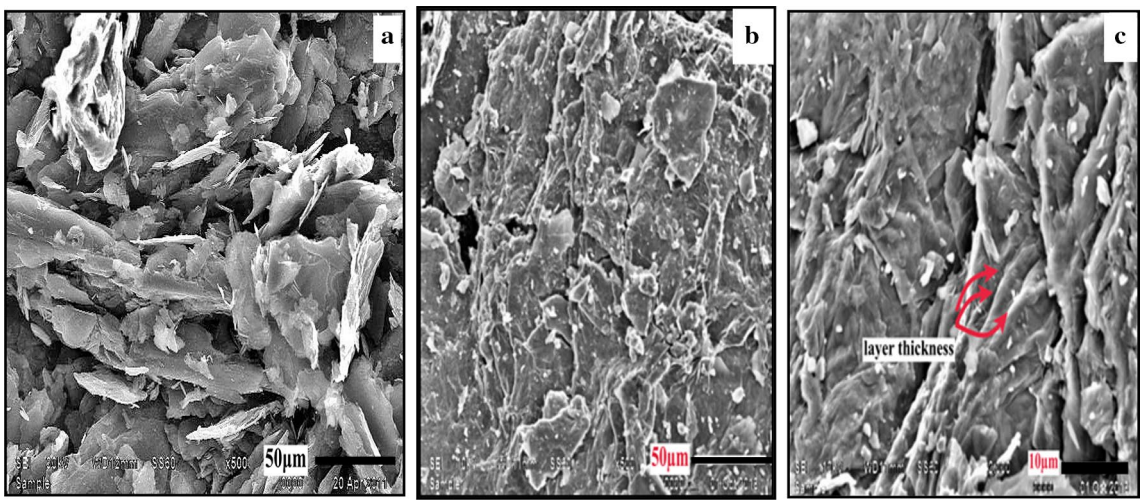

Fig. 2 **a** SEM of Graphite at 20 °C, **b, c** SEM of GO prepared by modified Hammer method at 20 °C

$$\%R = \left(\frac{C_{\text{des}}}{C_{\text{ads}}}\right)100\%, \tag{16}$$

where C_{ads} (mg L^{-1}) is the concentration of the studied $^{152+154}$Eu radioisotope in the solid phase, and C_{des} (mg L^{-1}) is the concentration of the $^{152+154}$Eu radioisotope in the aqueous phase.

Results and Discussion

Characterization of the Prepared Materials

FTIR-Analysis

Figure 1 shows a variety of oxygen derivatives functional group characteristics of GO. The strong wide peak at 3427 cm^{-1} was assigned to stretching vibration of O–H functional group due to physically adsorbed water, phenolic OH, or carboxylic group OH [27]. The two peaks with wave numbers 2923 and 2853 cm^{-1} correspond to C–H band of the hydrogen-bonded OH groups of dimeric COOH groups and intra-molecular-bonded O–H stretching of alcohols [28]. The bond with a wave number of ~ 1720 cm^{-1} related to stretching vibrations in the C=O bond of aldehyde, ketone, carboxyl, and ester functional groups where the vibration band at 868 cm^{-1} C–O–C deformation vibrations in epoxy groups [27]. Further, the intense bands at ~ 1653 cm^{-1} and 1566 cm^{-1} are related to the overlapping of the C=O stretching with in-phase N–H bonding, and overlapping of N–H bonding with the C–N stretching vibration [29].

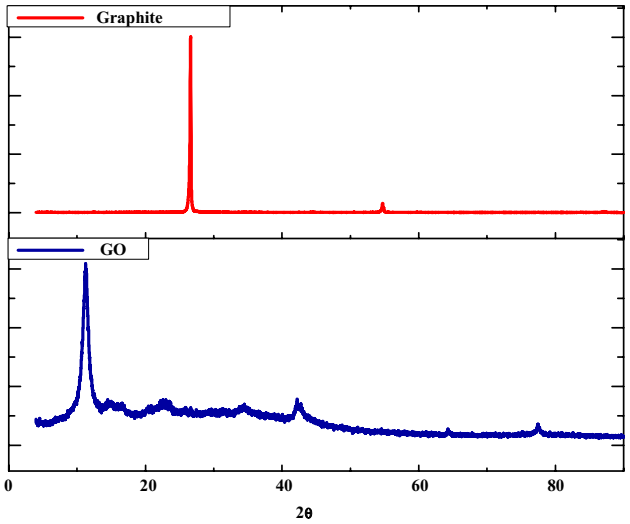

Fig. 4 X-ray diffraction of Graphite at 20 °C, and X-ray diffraction of GO prepared by modified Hammer method at 20 °C

SEM Analysis

The graphite micrograph seen in Fig. 2a indicates that the graphite has a platelet-like crystalline form of carbon [30]. The morphology of GO prepared by the modified Hammer method from pure natural graphite powder depicted in Fig. 2b,c shows aggregated crumpled layers structure [28]. The surface is smooth with wrinkles and folded regions [27]. The layer thickness is about 1 µm attributed to the introduction of the oxygen-containing functional groups [31].

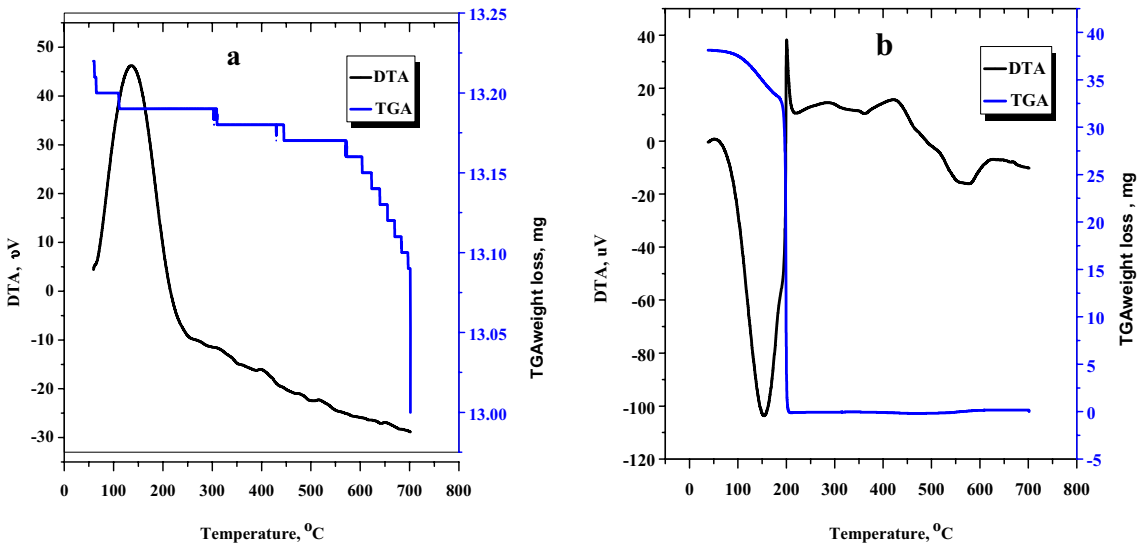

Fig. 3 **a** DTA-TGA of Graphite, **b** DTA-TGA of GO prepared by modified Hammer method

Thermal Investigations

Figure 3a and b depicts the DTA-TGA of graphite and GO. Figure 3a illustrates the thermal stability of graphite where the total weight loss is 0.99% with an endothermic peak at 134.5 °C due to loss of the physically adsorbed water. Figure 3b shows that graphene oxides have three stages for weight loss. The 1st stage of weight loss (12.88%) occurred at temperature 50–153 °C with an endothermic peak due to removal of adsorbed water, the 2nd stage occurs at 201 °C with weight loss (0.66%) accompanied with an exothermic peak due to secession of CO_2 from the oxygen-containing functional groups. Finally, the thermal decomposition (~86%) at 569 °C was mainly due to the combustion of the carbon skeleton [32].

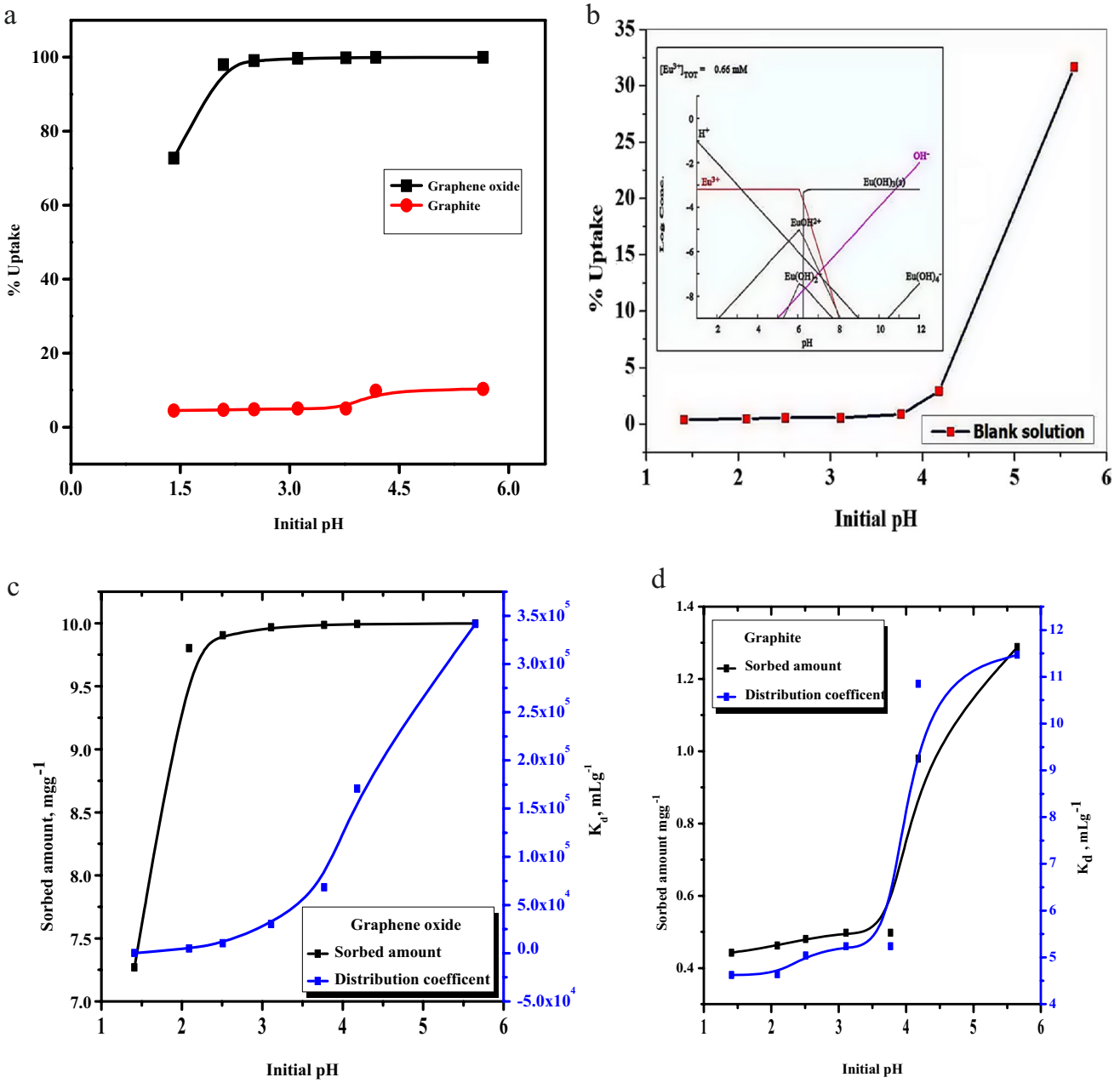

Fig. 5 Influence of pH on **a** Uptake percentage. **b** Precipitation curve, speciation diagram (inserted). **c** Sorbed amount and distribution coefficient of GO. **d** Sorbed amount and distribution coefficient of graphite for sorption of $^{152+154}$Eu onto graphene oxide and graphite [C_o of Eu = 100 mg L^{-1}, Contact time = 24 h, Temp. = 20 °C]

X-ray Diffraction

Figure 4 elucidates the XRD patterns of graphite and graphene oxide**.** Graphite shows a characteristic sharp peak at $2\theta = 26.7^{o}$, 55^{o} corresponding to hexagonal planes (002) and (004), respectively [28]. These planes confirmed the presence of well-arranged layer [30]. After the introduction of oxygen functionalities in GO, the crystallinity changed and the $2\theta = 26.7^{o}$ peak for graphite shifted to smaller angles $2\theta = 10.5^{o}$ [33].

Surface Characteristics

The surface characteristics results contribute to the sorption efficiency as the total pore area is 17.7 $m^2\ g^{-1}$ and the porosity measured a percentage of 25% of GO suitable for the sorption criteria. Sorption performance is closely related to the presence of macropores as the average pore diameter is 64.2 nm, more than 50 nm [34]. The presence of macrospores allows increased diffusion in the porous channels, resulting in greater sorption efficiency [35]. The presence of mesopores is responsible for the cracking of the surface. The apparent density is 1.2065 g L^{-1} and the bulk density of 0.8982 g L^{-1}. The bulk density takes into account the volume of the sample of GO and the open and the closed pores; the apparent density considers the volume of the GO sample and the closed pores only. The difference between the apparent density and the bulk density is an evidence for the existence of open pores [36].

Sorption Study

Influence of pH

Hydrogen ion concentration $[H^+]$ plays an important role in the sorption process of $^{152+154}$Eu onto graphene oxide (GO). The effect of the pH change on the sorption of 100 mg L^{-1} of $^{152+154}$Eu onto GO and its precursor graphite was studied in a pH range of 1–5.5. The results are represented in Fig. 5. The uptake percent increases from 73% to an ultimate value 99% of graphene oxide as pH rises from 1.5 to 5.5. (Fig. 5a). The sorbed amount as well as the distribution coefficients of $^{152+154}$Eu onto graphene oxide (GO) and graphite are represented in Fig. 5c and d, respectively. The sorbed amount and distribution coefficient increase as pH rises for graphene oxide. While the sorbed amount and distribution coefficient have no change with increase in the pH of graphite. This is due to the decrease in the competition of $[H^+]$, as at low pH, GO prefers to adsorb $[H^+]$ rather than $^{152+154}$Eu [37]. For the graphite precursor, the uptake percent is very low ~ 4.5% up to pH 4 due to the hydrophobic character of graphite [38]. Thus, graphite repels water solution and consequently decreases sorption of $^{152+154}$Eu radionuclide. Starting from pH 4, the uptake percent of $^{152+154}$Eu radionuclides onto graphite increased from 4.5 to 9% at pH 5.6 due to precipitation of Eu (III) [39].

The speciation diagram of Eu(III) at different pH values in an aqueous solution was studied with the aid of Hydra/Medusa chemical equilibrium software [40] and is depicted in Fig. 5b (inserted). Eu(III) dominates species up to pH 2.09 while $Eu(OH)_2^+$ and $Eu(OH)_4^-$ species dominant at pH greater than 2.09. At pH near a neutral solution and alkaline solution, $Eu(OH)_3$ is the dominant species[39].

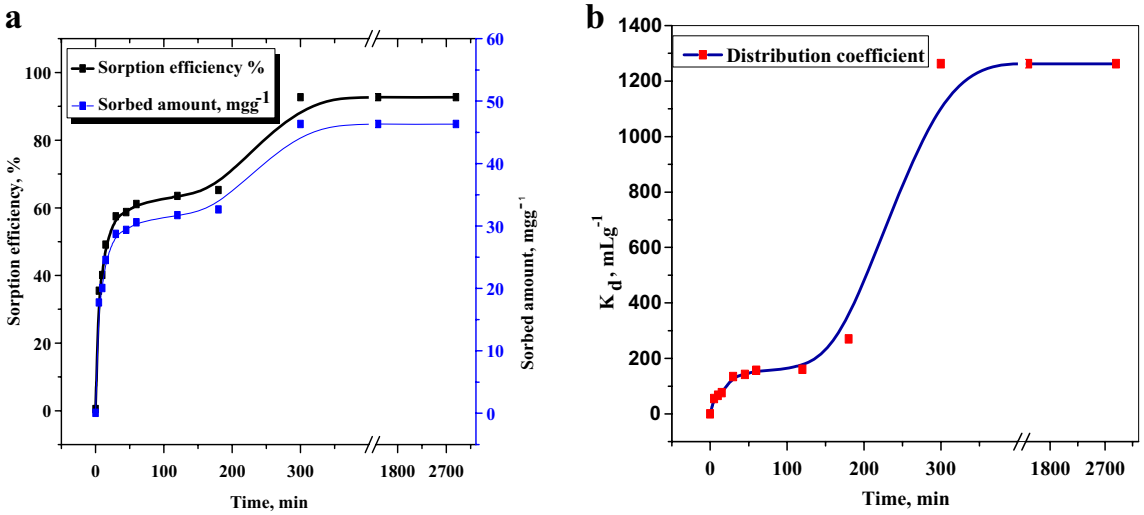

Fig. 6 Influence of contact time on: **a** Sorption efficiency %, and sorbed amount (mg g^{-1}). **b** Distribution coefficient for sorption of $^{152+154}$Eu onto graphene oxide [C_o of Eu = 500 mg L^{-1}, Temp. = 20 °C, pH 2.09]

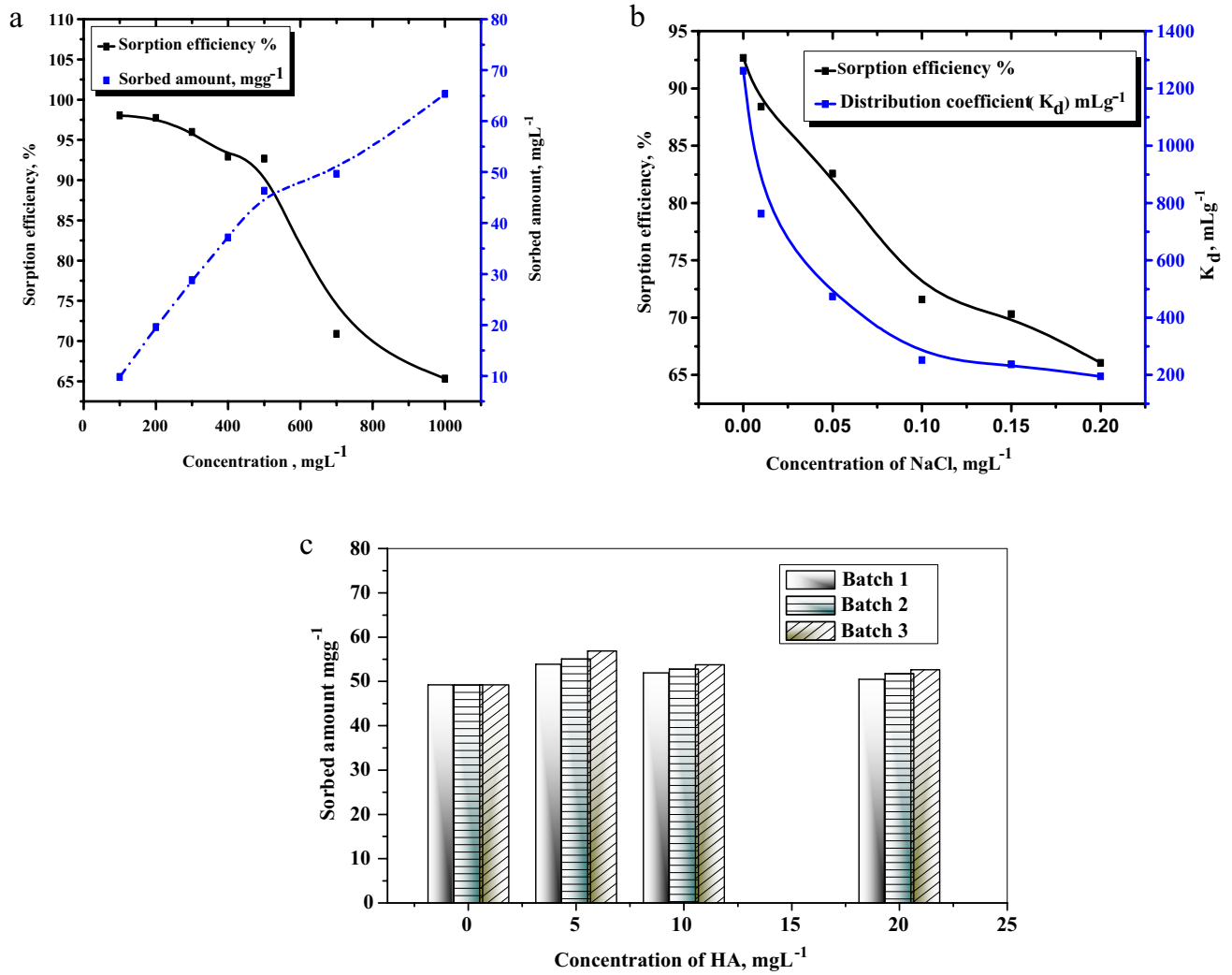

Fig. 7 **a** Influence of initial metal ion concentration on sorption efficiency %, and sorbed amount (mg g^{-1}). **b** Effect of ionic strength with initial concentration of Eu(III) 500 mg L^{-1}. **c** Effect of humic acid concentration with initial concentration of Eu(III) 700mg L^{-1} for sorption of $^{152+154}$Eu onto graphene oxide [V/m = 0.1 L g^{-1}, Temp. = 20 °C, pH 2.09, equilibrium time = 5 h]

The precipitation curve depicted in Fig. 5b shows an uptake percentage of $^{152+154}$Eu radionuclide increase for the blank solution of 3% at pH ≥ 4 and reaches 31.6% at pH 5.5. This increase in percentage is attributed to the $Eu(OH)_3$ species. All future sorption experiments will be executed at initial pH 2.09. The sorbed amounts of $^{152+154}$Eu onto graphene oxide and graphite at pH 2.09 are 9.8 mg g^{-1} and 0.461 mg g^{-1}, respectively.

Effect of Contact Time

The study of the effect of contact time on the sorption efficiency could enhance the suggestion of the kinetic mechanism of the sorption reaction. The plot of contact time within intervals (5–2880 min) of $^{152+154}$Eu radionuclide solution onto GO against sorption efficiency and sorbed amount (q_t) is depicted in Fig. 6a. Furthermore, the effect of $^{152+154}$Eu radionuclide solution's contact time onto GO against the distribution coefficient (K_d) of the $^{152+154}$Eu radionuclide is shown in Fig. 6b. As the time increases, the sorbed amount, sorption efficiency, and distribution

coefficient increase rapidly up to 100 min, then slowly up to equilibrium time at 5 h. The rapid increase of the sorbed amount is owing to the numerous available active sites of oxygen functional groups and/or binding sites which have relatively large activation energies found on the surface of graphene oxide [41, 42]. The slowdown of the sorbed amount near the equilibrium time is due to filling of the reactive sites and sorption of the metal ion on the less reactive sites followed by the diffusion into micropore sites [43]. The behavior of the $^{152+154}$Eu radionuclide sorption onto GO is relative to chemical sorption or surface complexation rather than physical adsorption [43].

Effect of Metal Ion Concentration

Variation of initial concentration Eu (III) solution from 100 to 1000 mg L^{-1} before spiking with $^{152+154}$Eu radioactive has a tangible effect on the sorption of $^{152+154}$Eu radionuclide onto GO. Figure 7a illustrates the plot of the initial concentration of $^{152+154}$Eu radionuclide against the sorption efficiency percentage and sorbed amount onto GO at pH 2.09 and 20 °C. As the initial concentration of $^{152+154}$Eu increases from 100 to 1000 mg L^{-1}, the sorption efficiency percentage decreases from 98 to 65%. Nevertheless, the increase in initial metal ion concentration leads to an increase in the sorbed amount from 9.8 to 65 mg g^{-1}. This is due to the sufficient available active sites of fixed dosage of GO at low concentrations of Eu(III), while these active sites are limited and have a less sorption efficiency [44].

Effect of Ionic Strength

Figure 7b shows the effect of ionic strength on the sorption reaction of $^{152+154}$Eu onto graphene oxide. The sorption efficiency percentage and distribution coefficient decrease with increasing concentration of NaCl due to competition of sorption between Na(I) and Eu (III). This indicates the sorption of $^{152+154}$Eu radionuclide onto GO depending on ionic strength. Therefore, the sorption of $^{152+154}$Eu radionuclide onto GO occurs due to complexation or ion exchange through the outer surface of oxygen functional groups on graphene oxide [43, 45, 46].

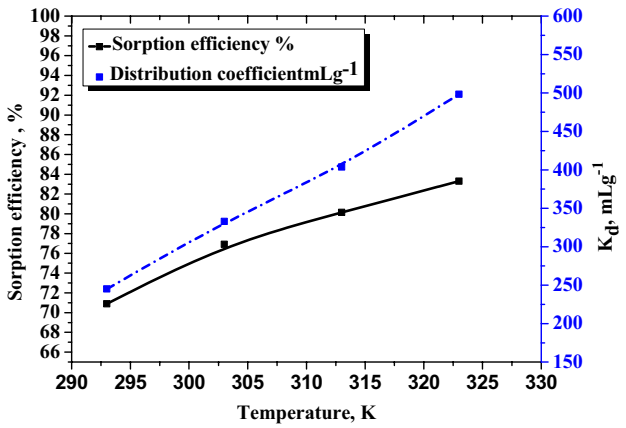

Fig. 8 Effect of temperature on the sorption of $^{152+154}$Eu radionuclide onto GO [C_o = 700 mg L^{-1}, pH 2.09, equilibrium time = 5 h]

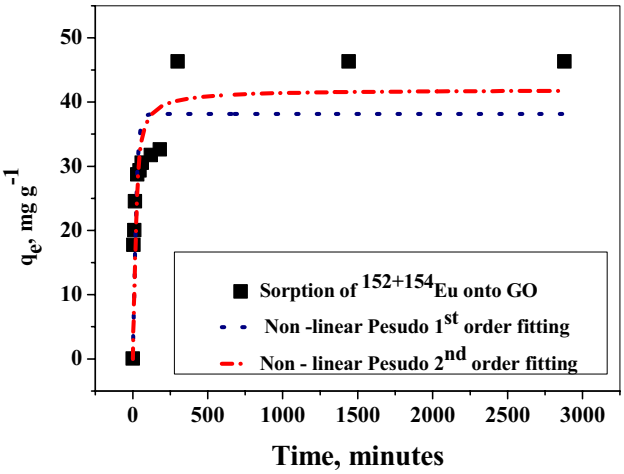

Fig. 9 Non-linear pseudo-1st-order and pseudo-2nd-order fitting for $^{152+154}$Eu radionuclide sorption onto GO [C_o of Eu = 500 mg L^{-1}, V/m = 0.1 L g^{-1}, Temp. = 20 °C, pH 2.09]

Effect of Humic Acid (HA)

In the aquatic environment, humic acid is a natural complexing agent found in natural waters and is considered to be one of the potential agents influencing the sorption behavior of long-lived radionuclides [47].

Figure 7c shows the sorption of $^{152+154}$Eu radionuclide onto GO as a function of humic acid (HA) initial concentration at pH 2.09 and room temp. 20 °C. Three batches were studied with different addition sequences that were studied: batch 1 spiking Eu(III) into the HA solution and then adding GO after 2 days, batch 2 spiking Eu(III) into the GO and then adding HA after 2 days, and batch 3 spiking HA into the GO and then adding Eu(III) after 2 days. The sorbed amount of $^{152+154}$Eu radionuclide onto GO increases from 49.23 mg g^{-1} to 53.86, 55.06, and 56.84 mg g^{-1} for batch 1, batch 2, and batch 3, respectively by adding 5 mg L^{-1} of humic acid. This is because of the sorption of humic acid on graphene oxide and, consequently, the surface adsorbed HA can form stronger stable complexes with $^{152+154}$Eu compared to that complexes formed with the functional groups on GO without humic acid [48], and thereby the sorption of $^{152+154}$Eu increases. By increasing the concentration of HA from 5 to 20 mg L^{-1}, the sorption of $^{152+154}$Eu radionuclide

Table 1 Calculated parameters of the non-linear pseudo-1st-order and pseudo-2nd-order kinetic models fitting for $^{152+154}$Eu radionuclide sorption onto GO

Temperature (°C)	Pseudo-1st-order kinetic parameters			$q_{e\,(exp)}$ mg g^{-1}	Pseudo 2nd order kinetic Parameters		
	k_1 min^{-1}	$q_{e\,(cal.)}$ mg g^{-1}	R^2		k_2 ($\times 10^{-3}$) (g mg^{-1} min^{-1})	$q_{e\,(cal.)}$ mg g^{-1}	R^2
20 °C	0.0642	38.1345	0.76	46.33	1.9	41.92	0.87

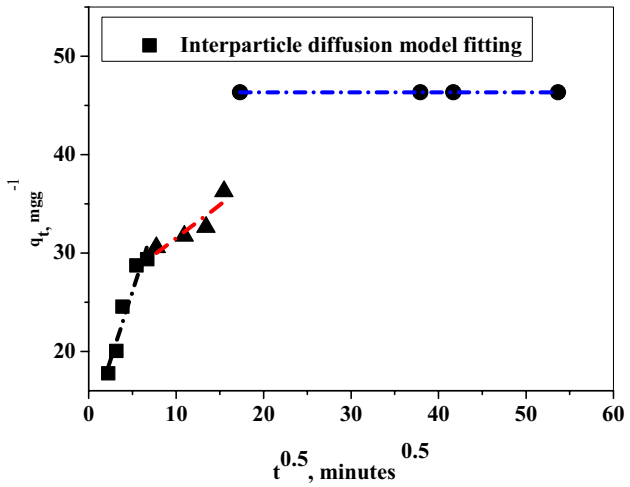

Fig. 10 Intraparticle diffusion model fitting for $^{152+154}$Eu radionuclide sorption onto GO [C_o of Eu = 500 mg L^{-1}, V/m = 0.1 L g^{-1}, Temp. = 20 °C, pH 2.09]

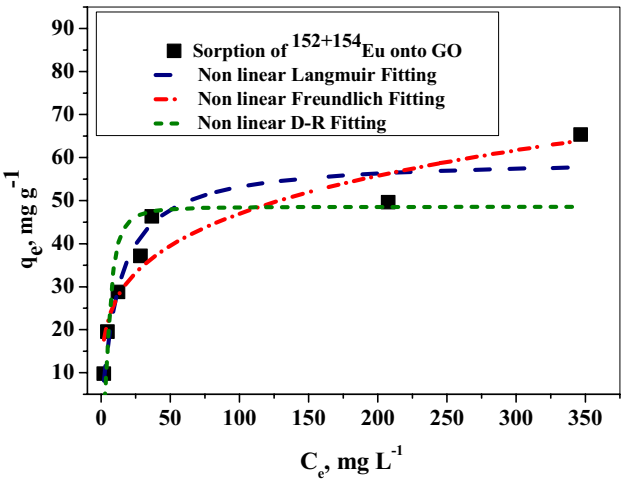

Fig. 11 Non-linear isotherm modeling fitting for $^{152+154}$Eu radionuclide sorption onto GO [V/m = 0.1 L g^{-1}, Temp. = 20 °C, pH 2.09, equilibrium time = 5 h]

Table 2 Diffusion model parameters for $^{152+154}$Eu radionuclide sorption onto GO at 20 °C

Intraparticle diffusion model			
Time range, min	K_{id}, (g mg^{-1} min^{-1})	C	R^2
1–45	3.501 ± 0.44	9.85 ± 1.698	0.95
60–240	0.45 ± 0.44	26.66 ± 0.73	0.93
300–2880	–	46.33	–

on HA-GO decreased. This is may be due to the GO particle's pores blocked at a high concentration of HA [49]. The sorbed amounts of $^{152+154}$Eu radionuclide increase in the order batch 3 > batch 2 > batch 1. This voted for sorption of $^{152+154}$Eu radionuclide is influenced by the addition sequence 3 where HA was first adsorbed on GO, and then $^{152+154}$Eu radionuclide was sorbed to HA-GO surface as a result of the stability of the $^{152+154}$Eu radionuclide onto HA-GO [48].

Effect of Temperature

The sorption of $^{152+154}$Eu radionuclide onto GO is temperature dependent, as shown in Fig. 8. The sorption efficiency as well as the distribution coefficient increases as the temperature increases. This is an interpretation of the endothermic nature of $^{152+154}$Eu radionuclide sorption to GO.

Kinetic Modeling

Figure 9 represents the non-linear plots of Eqs. (4, 5) for pseudo-1st order and pseudo-2nd order, respectively. The kinetic parameters are listed in Table 1. R^2 (correlation factor) of the pseudo-2nd order (0.87) is more than R^2 of the pseudo-1st order (0.76) which gives a possibility for the pseudo-2nd-order mechanism suitability for the sorption reaction. Also, the value of $q_{e\,(cal.)}$ resembles the experimental data of $q_{e\,(exp.)}$ ensuring that the mechanism of the sorption reaction is more adequately described by the pseudo-2nd-order model, and a chemical reaction/chemisorption or ion exchange is assumed to be the rate-controlling step [50, 51].

Figure 10 shows the interparticle diffusion plot fitting**.** A two-linear region followed by a plateau is present in the plot. In the plot, the first region (fast step) from 1 to 45 min involves the mass transfer of metal ions from the bulk of the solution to the surface of graphene oxide. The second region (slow step) from 60 to 240 min expresses the diffusion of metal ions to the active sites of graphene oxide, and this is the rate-determining step. The third one is the saturation

Table 3 Calculated parameters of the non-linear isotherm modeling parameters for $^{152+154}$Eu radionuclide sorption onto GO

Temp. (°C)	Langmuir isotherm model			Freundlich isotherm model			D-R isotherm model		
	q_m (mg g^{-1})	b	R^2	K_f (mg g^{-1})	n	R^2	q_m (mg g^{-1})	β	R^2
20 °C	59.81	0.080	0.92	14.95	4.023	0.88	48.575	31.51	0.66

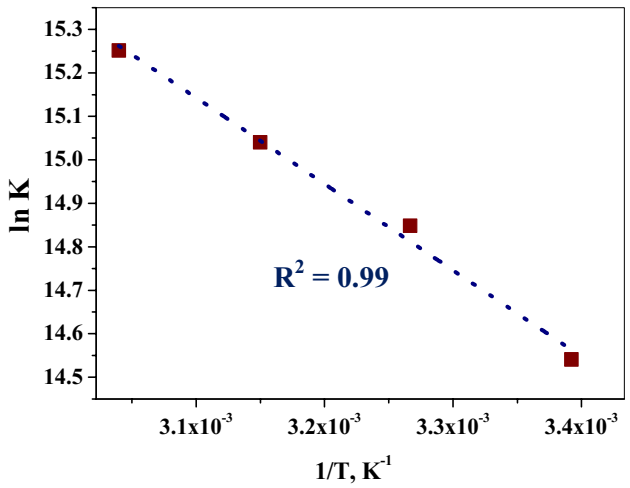

Fig. 12 Van't Hoff plot for fitting for $^{152+154}$Eu radionuclide sorption onto GO [C_o of Eu = 700 mg L^{-1}, V/m = 100 mL g^{-1}, pH 2.09, equilibrium time = 5 h]

step, started from 5 h [52]. Table 2 includes the intraparticle diffusion coefficients of K_{id} calculated by Eq. (6).

Isotherm Modeling

The sorption process was examined for Langmuir, Freundlich, and D-R isotherm models. The non-linear plots are depicted in Fig. 11, and the calculated parameters of the applied parameters are listed in Table 3. Model selection is based on the highest R^2 values (highest correlation factor). The results showed that the order of the correlation coefficients R^2 for the applied models is Langmuir > Freundlich > D–R model. Therefore, the sorption of $^{152+154}$Eu radionuclide sorption onto GO could be regulated by the Langmuir isotherm model. The monolayer capacity of $^{152+154}$Eu radionuclide sorption onto GO is 59.81 mg g^{-1} and the calculated R_L value is 0.0244 within the range $0 < R_L < 1$ which refers to favorable sorption reaction.

Table 4 Thermodynamic parameters for the sorption of $^{152+154}$Eu radionuclide sorption onto GO

ΔG^o, KJ mol^{-1}				ΔH^o kJ mol^{-1}	ΔS^o, J mol^{-1} K^{-1}
293 K	303 K	313 K	323 K		
− 35.504	− 37.340	− 39.177	− 41.013	18.307 ± 130.8	183.6562 ± 0.42

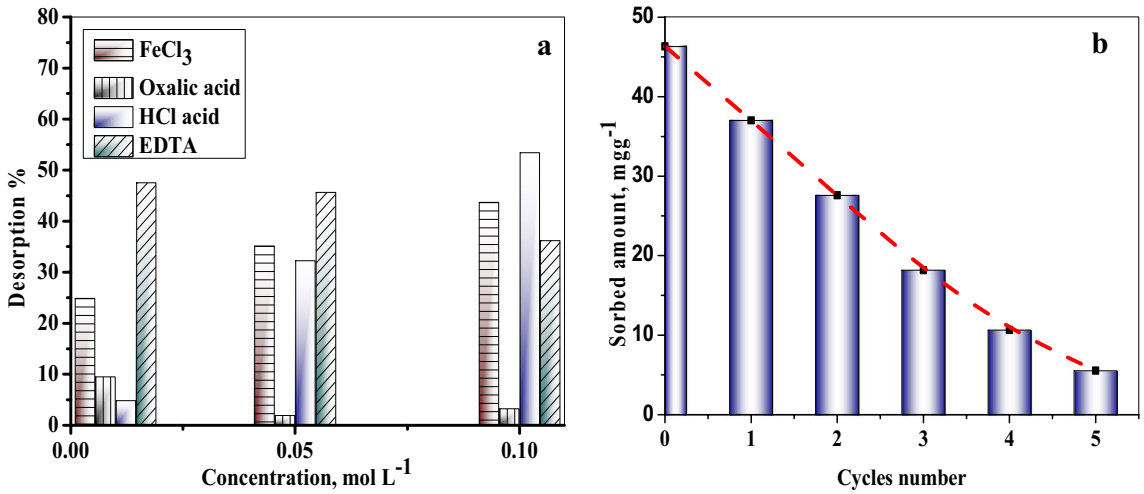

Fig. 13 **a** Desorption study of $^{152+154}$Eu radionuclide-loaded GO. **b** Reusability of GO for sorption of $^{152+154}$Eu using 0.1 mol L^{-1} HCl [C_o = 500 mg L^{-1}, pH 2.09, desorbing time = 24 h, temperature = 20 °C]

Thermodynamic Studies

Thermodynamic parameters such as enthalpy (ΔH^o), entropy (ΔS^o), and Gibbs free energy (ΔG^o) are other important factors for the sorption reaction. The calculated parameters of the sorption studies were calculated from the slope and intercept of the plot in Fig. 12, ln K (corrected equilibrium constant) as a function of $1/T$. ΔH^o, ΔS^o, and ΔG^o at different temperatures represented in Table 4 showed the spontaneous sorption reaction of $^{152+154}$Eu radionuclide onto GO. As the temperature is raised, the ΔG^o negativity values increase indicating the endothermic nature [53] of the sorption reaction. This is besides the positive sign of ΔH. The value of (ΔS^o) is positive that means increase in the disorder at the surface of GO. This reveals the ability of GO surface toward $^{152+154}$Eu sorption to cause a structural change in GO and $^{152+154}$Eu radionuclide during the process. The increase in entropy is a result of an increase in the disorder of the solid-solution system. This increase in the disorder of GO could be a result of the extra entropy of water molecules formed due to the $^{152+154}$Eu radionuclide replacement of [H^+] [54].

Desorption Studies and Reusability

The choice of an efficient sorbent not only depends on its sorption capacity but also depends on its ability to desorption [55], from a practical and an economic point of view. Figure 13a depicts three different concentrations of 0.01, 0.05, and 0.1 M from $FeCl_3$, oxalic acid, HCl, and EDTA solutions used for recovery of $^{152+154}$Eu loaded onto GO. The results show that 0.1 M HCl has a maximum desorption percentage and could be used as an efficient eluent for $^{152+154}$Eu radionuclide. The desorption percentage decreases by increasing the concentration of both EDTA and oxalic acid. This is due to the hindrance of the accumulated desorbed Eu /ligand as a result of larger sizes of metal–ligand complexes [56]. The order of the examined eluents is EDTA > $FeCl_3$ > HCl > oxalic acid for a low concentration (0.05 M). However, the order is HCl > $FeCl_3$ > EDTA > oxalic at a high concentration (0.1 M) of the eluents. The rise in desorption efficiency of $FeCl_3$ could be related to ion exchange between Fe (III) and Eu (III).

Also, the reusability controls the efficiency of the sorption process. It contributes to the determination of the total cost of the recovery process of RE^{3+}. The desorption agent used was a 0.1 M HCl solution, and the time for desorption

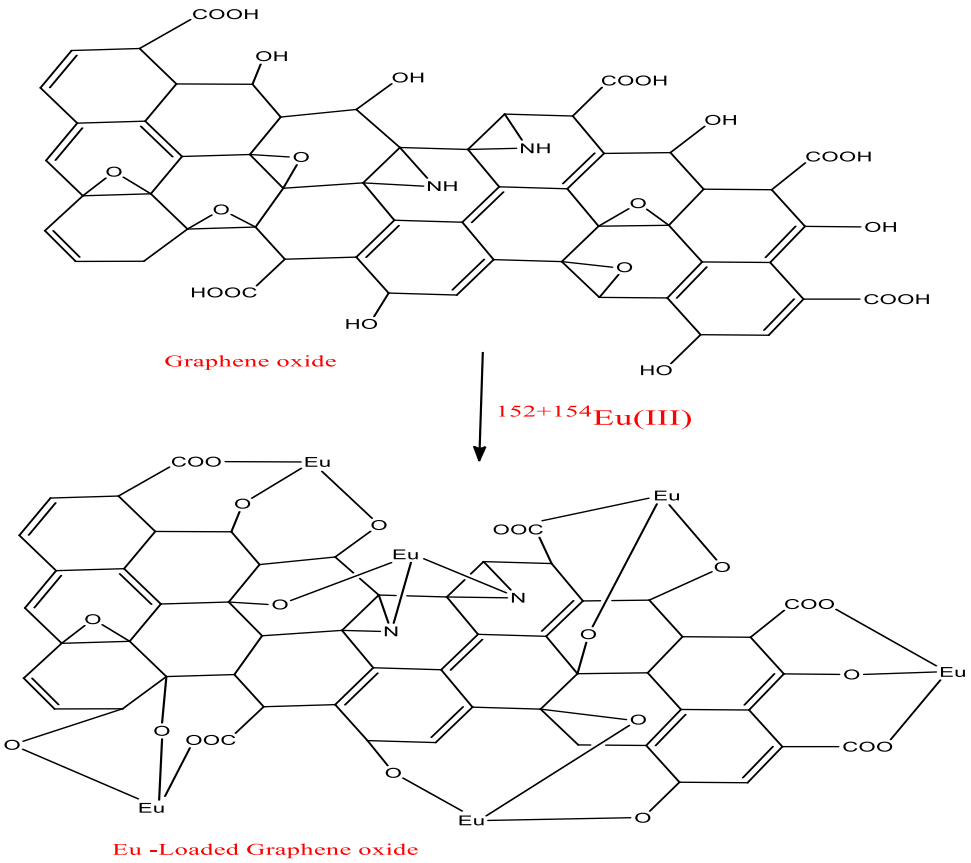

Fig. 14 Mechanism of sorption of $^{152+154}$Eu radionuclide onto GO [C_o = 500 mg L^{-1}, pH 2.09, Eq. time = 5 h, temperature = 20 °C]

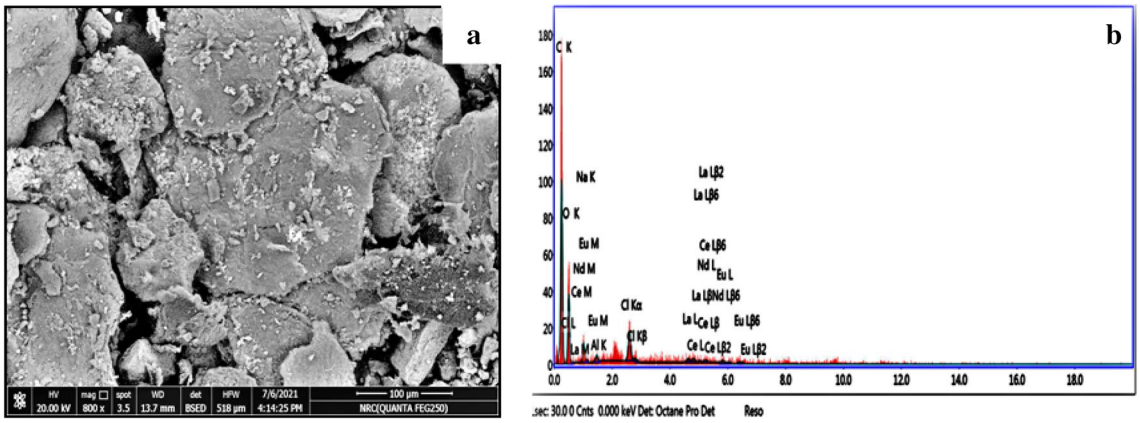

Fig. 15 **a** SEM of Loaded RE^{3+} onto GO. **b** EDX of Loaded RE^{3+} onto GO

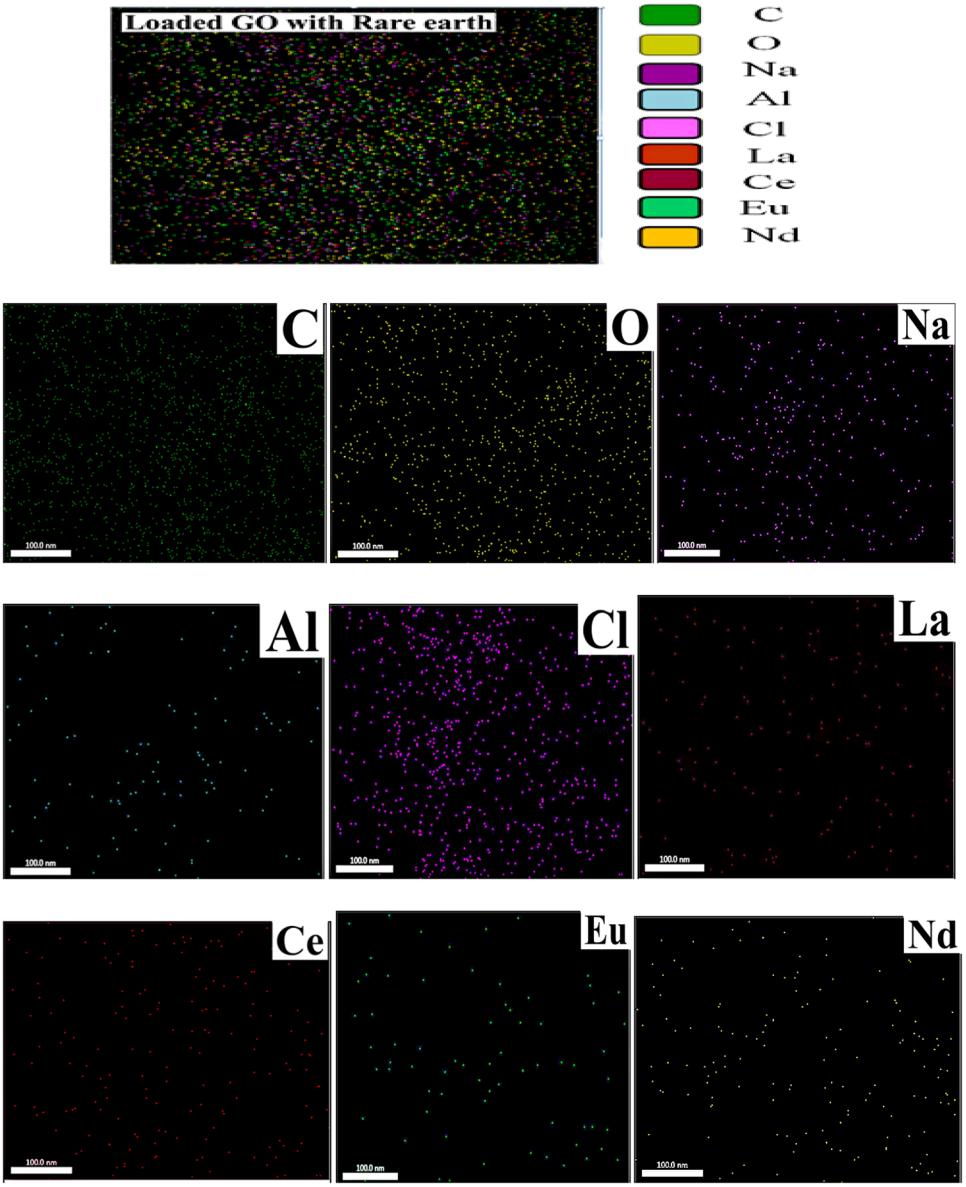

Fig. 16 EDX Mapping image of loaded RE^{3+} onto GO

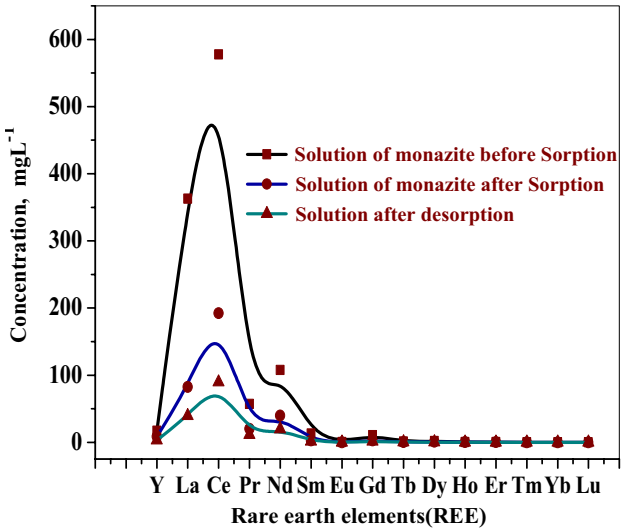

Fig. 17 Concentration of rare-earth ions (RE^{3+}) liquor from monazite: before and after sorption onto GO and after desorption of RE^{3+} ions by 0.1 mol L^{-1} HCl eluent at 20 °C

was 24 h. The reusability performance (adsorption–desorption–adsorption) is represented in Fig. 13b. The sorption capacity of GO decreased after the first cycle from 46.32 to 37.01 mg $g^{-1}$with ~ 21% decrease in the sorption efficiency. After the second cycle, the sorption capacity decreased from 37.01 to 27.59 mg g^{-1} and then further decreased in 18.17, 10.64, and 5.54 mg g^{-1} in the third, fourth, and fifth cycles, respectively. The decrease in the sorbed amount is related to the decrease of the available active sites, and thus, accounts for both ion exchange and the covalent bonding between $^{152+154}$Eu (III) and GO in the sorption mechanism and confirms the chemisorption of the Langmuir isotherm model and the pseudo-2nd-order kinetic model.

Mechanism of Sorption Process

$^{152+154}$Eu(III) adsorbed onto the surface of GO through oxygenated functional groups –COOH, –OH, –O–, and through amide groups, –NH as shown in Fig. 14.

Recovery of Rare Earth Elements from Monazite

Sorption of RE^{3+} onto graphene oxide was performed by shaking 10 mL of the liquor monazite-digested solution for 5 h at 20 °C with 0.1 g of the GO and pH adjusted at 2.09. The loaded GO with REEs ions (Fig. 15a) shows a rough surface compared to GO before sorption in Fig. 2 b and c. The results are confirmed with the aid of energy-dispersive X-ray spectra (Fig. 15b.) Besides carbon and oxygen bonds, the main constituents of graphene oxide, the spectrum shows Lanthanum (La), Cerium (Ce), Neodymium (Nd), Europium (Eu) bonds in addition to Chlorine (Cl), Sodium (Na), and Aluminum (Al) consistent with the elemental formula of monazite.

The mapping image of loaded GO in Fig. 16 proved the sorption of REEs onto GO. La, Ce, Nd, and Eu are taken as examples of REEs to confirm the sorption process. Figure 17 clarifies the concentration of RE^{3+} (mg L^{-1}) before and after the sorption process as well as the concentration of desorption RE^{3+} performed. The sorption efficiencies are shown in Table 5. Furthermore, GO shows selectivity for RE^{3+} where the sorption efficiency of RE^{3+} is different and ranged from a maximum 82.75% for Yb^{3+} to 51% for Y^{3+}. These differences in sorption efficiency may be owing to their difference in ionic size.

The RE3 + recovery was obtained by treatment-loaded graphene oxide with 0.1 mol L^{-1} HCl for 24 h. The recovery percentage is shown in Table 5. The recovery percentage results showed the possibility to retain REEs from monazite leachate. The recovery ratios of REEs metal ions have nearly similar values.

Conclusion

Graphene oxide (GO) is prepared by the Hammers method. FTIR analysis indicates the presence of oxygenated groups such as C=O, O–H, and COO that are responsible for its sorption efficiency, in addition to the porosity of GO which was found, to be 25%. The sorption parameters were

Table 5 Sorption efficiency of RE^{3+} onto GO and recovery percentage by 0.1 mol L^{-1} HCl eluent

REEs Ion	Sorption %	Recovery %	REEs ion	Sorption %	Recovery %
Yttrium (Y)	51.14	33.2	Terbium (Tb)	71.81	18.63
Lanthanum (La)	77.26	14.1	Dysprosium (Dy)	69.85	19.77
Cerium (Ce)	66.69	23.22	Holmium (Ho)	65.95	22.41
Praseodymium (Pr)	64.97	30.57	Erbium (Er)	65.17	22.62
Neodymium (Nd)	63.014	29.08	Thulium (Tm)	64.22	22.78
Samarium (Sm)	79.89	13.69	Ytterbium (Yb)	82.75	9.76
Europium (Eu)	74.92	16.72	Lutetium (Lu)	65.75	21.46
Gadolinium (Gd)	72.71	17.77			

optimized to be at pH 2.09, and the equilibrium time was achieved after 5 h. The sorption reaction kinetic mechanism is regulated with pseudo-2nd order implying that chemisorption reaction is expected. The sorption reaction is satisfied with the Langmuir model, confirming the chemisorption reaction. The monolayer capacity of $^{152+154}$Eu (III) onto GO at 20 °C is 59.81 mg g^{-1}. With desorbing efficiency 53.42%, 0.1 M HCl is used as eluent for $^{152+154}$Eu (III). The reusability studies show the decrease in the sorbed amount due to the decrease in the available active sites which indicates both ion exchange and covalent bonding between $^{152+154}$Eu (III) and GO in the sorption mechanism and confirms chemisorption of the Langmuir isotherm model and the pseudo-2nd-order kinetic model.

The adsorbed GO has sorption selectivity for RE^{3+} and could be used in separation as the sorption efficiency for Y^{3+} is 51.14% and for Yb^{3+} is 82.75%. The sorption reaction is spontaneous and favorable. As the recovery percentage of RE^{3+} is only 20.1%, The authors decided to use poly ethylene glycol and Agricultural waste products with GO as a prospective composite in a further study to improve the layer structure of GO, raise the porosity of GO and, consequently, increase the sorption efficiency.

Author Contributions EES, SM, and GD contributed to the study conception and design, Material preparation, data collection, and analysis. All authors read and approved the final manuscript.

Funding Open access funding provided by The Science, Technology & Innovation Funding Authority (STDF) in cooperation with The Egyptian Knowledge Bank (EKB). The authors received no financial support for the research, authorship, and/or publication of this article.

Declarations

Conflict of interest The authors declare that they have no conflict of interest.

References

1. Amer TE, Abdella WM, Wahab GMA et al (2013) A suggested alternative procedure for processing of monazite mineral concentrate. Int J Min Process 125:106–111. https://doi.org/10.1016/j.minpro.2013.10.004
2. Preinfalk C, Morteani G (1989) The industrial applications of rare earth elements. In: Möller P, Černý P, Saupé F (eds) Lanthanides, tantalum and niobium. Special publication No. 7 of the Society for Geology Applied to Mineral Deposits, vol 7. Springer, Berlin
3. Balaram V (2019) Rare earth elements: a review of applications, occurrence, exploration, analysis, recycling, and environmental impact. Geosci Front 10:1285–1303. https://doi.org/10.1016/j.gsf.2018.12.005
4. Belova VV (2017) Development of solvent extraction methods for recovering rare earth metals. Theor Found Chem Eng 51:599–609. https://doi.org/10.1134/S00405795160502X
5. Güneş H, Obuz HE, Alkan M (2019) Selective precipitation of Th and rare-earth elements from HCl Leach Liquor. Rare Metal Technol. https://doi.org/10.1007/978-3-030-05740-4_9
6. Kim D, Powell LE, Delmau LH et al (2015) Selective extraction of rare earth elements from permanent magnet scraps with membrane solvent extraction. Environ Sci Technol 49:9452–9459. https://doi.org/10.1021/acs.est.5b01306
7. Xie F, An Zhang T, Dreisinger D et al (2014) A critical review on solvent extraction of rare earths from aqueous solutions. Miner Eng 56:10–28. https://doi.org/10.1016/j.mineng.2013.10.021
8. Maes S, Zhuang WQ, Rabaey K et al (2017) Concomitant leaching and electrochemical extraction of rare earth elements from monazite. Environ Sci Technol 51:1654–1661. https://doi.org/10.1021/acs.Est.6b03675
9. Hovey JL, Dardona M, Allen MJ et al (2021) Sorption of rare-earth elements onto a ligand-associated media for pH-dependent extraction and recovery of critical materials. Sep Purif Technol 258:118061. https://doi.org/10.1016/j.seppur.2020.118061
10. Ashour RM, Abdelhamid HN, Abdel-Magied AF et al (2017) Rare earth ions adsorption onto graphene oxide nanosheets. Solvent Extr Ion Exch 35:91–103. https://doi.org/10.1080/07366299.2017.1287509
11. Li M, Ji Z, Sheng G et al (2021) Scavenging mechanism of rare earth metal ions in water by graphene oxide. J Mol Liq 322:114940. https://doi.org/10.1016/j.molliq.2020.114940
12. Smith AT, LaChance AM, Zeng S et al (2019) Synthesis, properties, and applications of graphene oxide/reduced graphene oxide and their nanocomposites. Nano Mater Sci 1(1):31–47. https://doi.org/10.1016/j.nanoms.2019.02.004
13. Kuilla T, Bhadra S, Yao D et al (2010) Recent advances in graphene based polymer composites. Prog Polym Sci 35(11):1350–1375. https://doi.org/10.1016/j.progpolymsci.2010.07.005
14. Chen Y, Xu P, Shu Z et al (2014) Multifunctional graphene oxide-based triple stimuli-responsive nanotheranostics. Adv Funct Mater 24:4386–4396. https://doi.org/10.1002/adfm.201400221
15. Catania F, Marras E, Giorcelli M et al (2021) A Review on recent advancements of graphene and graphene-related materials in biological applications. Appl Sci 11(2):614. https://doi.org/10.3390/app11020614
16. Zhao GX, Li JX, Ren XM et al (2011) Few layered graphene oxide nanosheets as superior sorbents for heavy metal ion pollution management. Environ Sci Technol 45:10454–10462. https://doi.org/10.1021/es203439v
17. Zaaba NI, Foo KL, Hashim U et al (2017) Synthesis of graphene oxide using modified hummers method: solvent Influence. Procedia Eng 184:469–477. https://doi.org/10.1016/j.proeng.2017.04.118
18. Brückner L, Elwert T, Schirmer T (2020) Extraction of rare earth elements from phospho-gypsum: concentrate digestion, leaching, and purification. Metals 10:131. https://doi.org/10.3390/met10010131

19. Dakroury GA, El-Shazly EAA, Hassan HS (2021) Sorption of lead (II) and strontium (II) ions from aqueous solutions onto non-living Chlorella Vulgaris Alga/Date pit activated carbon composite. Carbon Lett. https://doi.org/10.1007/s42823-021-00280-z
20. Dakroury GA, Abo-Zahra SF (2020) The use of titanium oxide/polyethylene glycol nanocomposite in sorption of ^{134}Cs and ^{60}Co radionuclides from aqueous solutions. J Radioanal Nucl Chem 324:1351–1364. https://doi.org/10.1007/s10967-020-07167-9
21. Dakroury GA, El-Shazly EAA, Hassan HS (2021) Preparation and characterization of ZnO/Chitosan nanocomposite for Cs(I) and Sr(II) sorption from aqueous solutions. J Radioanal Nucl Chem 330(1):159–174. https://doi.org/10.1007/s10967-021-07935-1
22. Abdel-Galil E, Ibrahim A, El-Kenany W (2021) Facile fabrication of a novel silico vanadate ion exchanger: evaluation of its sorption behavior towards europium and terbium ions. Desalin Water Treat. https://doi.org/10.5004/dwt.2021.27261
23. Jasper EE, Ajibola VO, Onwuka JC (2020) Nonlinear regression analysis of the sorption of crystal violet and methylene blue from aqueous solutions onto an agro-waste derived activated carbon. Appl Water Sci 10:132. https://doi.org/10.1007/s13201-020-01218-y
24. Yadav M, Singh NK (2017) Isotherm investigation for the sorption of fluoride onto Bio-F: comparison of linear and non-linear regression method. Appl Water Sci 7:4793–4800. https://doi.org/10.1007/s13201-017-0602-9
25. Uddin MK (2017) A review on the adsorption of heavy metals by clay minerals, with special focus on the past decade. Chem Eng J 308:438–462. https://doi.org/10.1016/j.cej.2016.09.029
26. Lima EC, Hosseini-Bandegharaei A, Moreno-Piraján JC et al (2019) A critical review of the estimation of the thermodynamic parameters on adsorption equilibria. Wrong use of equilibrium constant in the Van't Hoof equation for calculation of thermodynamic parameters of adsorption. J Mol Liq 273:425–434. https://doi.org/10.1016/j.molliq.2018.10.048
27. Sieradzka M, Ślusarczyk C, Biniaś W et al (2021) The role of the oxidation and reduction parameters on the properties of the reduced graphene oxide. Coatings 11:166–183. https://doi.org/10.3390/coatings11020166
28. Manoratne CH, Rosa SRD, Kottegoda IRM (2017) XRD-HTA, UV Visible, FTIR and SEM interpretation of reduced graphene oxide synthesized from high purity vein graphite. Mater Sci Res India 14:19–30. https://doi.org/10.13005/msri/140104
29. Luceño-Sánchez JA, Maties G, Gonzalez-Arellano C et al (2018) Synthesis and characterization of graphene oxide derivatives via functionalization reaction with hexamethylene diisocyanate. Nanomaterials 8(11):870–889. https://doi.org/10.3390/nano8110870
30. Hidayah NMS, Liu WW, Lai CW et al (2017) Comparison on graphite, graphene oxide and reduced graphene oxide: synthesis and characterization. AIP Conf Proc. https://doi.org/10.1063/1.5005764
31. Saleem H, Haneef M, Abbasi HY (2018) Synthesis route of reduced graphene oxide via thermal reduction of chemically exfoliated graphene oxide. Mater Chem Phys 204:1–7. https://doi.org/10.1016/j.matchemphys.2017.10.020
32. Suyambrakasam G, Muthiah P, Rajendran GR (2015) Synthesis and characterization of few layered graphene oxide prepared using chemical exfoliation method. Int J Appl Eng Res 10(59):350–356
33. Gascho JLS, Costa SF, Recco AAC et al (2019) Graphene oxide films obtained by vacuum filtration: X-Ray diffraction evidence of crystalline reorganization. J Nanomater. https://doi.org/10.1155/2019/5963148
34. Kang S, Yu JS, Kruk M et al (2002) Synthesis of an ordered macroporous carbon with 62 nm spherical pores that exhibit unique gas adsorption properties. Chem Commun 16:1670–1671. https://doi.org/10.1039/b204756j
35. Pohan NA, Wahid MH, Zainal Z et al (2021) Pickering-emulsion-templated synthesis of 3D hollow graphene as an efficient oil absorbent. RSC Adv 11:3963–3971. https://doi.org/10.1039/D0RA09265G
36. Erb DJ (2018) Study of pore development in silicon oxycarbide ceramics to understand the microstructural evolution, M.Sc. Thesis, Faculty of Virginia Polytechnic Institute and State University, Blacksburg, VA. https://vtechworks.lib.vt.edu/bitstream/handle/10919/84900/Erb_DJ_T_2018.pdf
37. Torab-Mostaedi M, Asadollahzadeh M, Hemmati A et al (2015) Biosorption of lanthanum and cerium from aqueous solutions by grapefruit peel: equilibrium, kinetic and thermodynamic studies. Res Chem Intermed 41:559–573. https://doi.org/10.1007/s11164-013-1210-4
38. Akhair SHM, Harun Z, Basri H et al (2018) Hydrophobicity properties of graphite and reduced graphene oxide of the polysulfone (PSf) mixed matrix membrane. Int J Eng 31:1381–1388
39. Kang MJ, Hahn PS (2004) Adsorption behavior of aqueous europium on kaolinite under various disposal conditions. Korean J Chem Eng 21:419–424. https://doi.org/10.1007/BF02705430
40. Puigdomenech I (2013) Make equilibrium diagrams using sophisticated algorithms (MEDUSA).Inorganic Chemistry, Royal Institute of Technology, Stockholm Sweden. http://www.kemi.kth.se/medusa. https://www.sites.google.com/site/chemdiagr/
41. Katubi KMM, Alsaiari NS, Alzahrani FM et al (2013) Synthesis of manganese ferrite/graphene oxide magnetic nanocomposite for pollutants removal from water. Processes 9:589. https://doi.org/10.3390/pr9040589
42. Li D, Zhang B, Xuan F (2015) The sorption of Eu(III) from aqueous solutions by magnetic graphene oxides: a combined experimental and modeling studies. J Mol Liq 211:203–209. https://doi.org/10.1016/j.molliq.2015.07.012
43. Chen Z, He J, Lu S et al (2016) Sorption and desorption properties of Eu(III) on attapulgite. J Radioanal Nucl Chem 307:1093–1104. https://doi.org/10.1007/s10967-015-4252-9
44. Swelam AA, Saied S, Hafez A (2019) Removal comparative study for Cd (II) ions from polluted solutions by adsorption and coagulation techniques using *Moringa oleifera* seeds. Egypt J Chem 62:1499–1517
45. Zhu B, Zhang Z, Song F et al (2020) Efficient removal of U(VI) ions from aqueous solutions by tannic acid/graphene oxide composites. Appl Sci 10:8870–8881. https://doi.org/10.3390/app10248870
46. Yao T, Xiao Y, Wu X et al (2016) Adsorption of Eu (III) on sulfonated graphene oxide: combined macroscopic and modeling techniques. J Mol Liq 215:443–448. https://doi.org/10.1016/j.molliq.2015.11.030
47. Jain A, Yadavb K, Mohapatraa M et al (2019) Spectroscopic investigation on europium complexation with humic acid and its model compounds. Spectrochim Acta A Mol Biomol Spectrosc 72:1122–1126. https://doi.org/10.1016/j.saa.2009.01.008
48. Chang P, Yu S, Chen T et al (2007) Effect of pH, ionic strength, fulvic acid and humic acid on sorption of Th (IV) on Na-rectorite. J Radioanal Nucl Chem 274:153–160. https://doi.org/10.1007/s10967-006-6865-5
49. Adeyinka GC, Moodley B (2019) Effect of aqueous concentration of humic acid on the sorption of polychlorinated biphenyls onto soil particle grain sizes. J Soils Sedim 19:1543–1553. https://doi.org/10.1007/s11368-018-2147-4
50. Hu B, Hu Q, Li X et al (2017) Rapid and highly efficient removal of Eu (III) from aqueous solutions using graphene oxide. J Mol Liq 229:6–14. https://doi.org/10.1016/j.molliq.2016.12.030
51. Rocha PD, Franca AC, Oliveira LS (2015) Batch and column studies of phenol adsorption by an activated carbon based on acid treatment of corn cobs. Int J Eng Technol 7:459–464. https://doi.org/10.7763/IJET.2015.V7.837

52. Tsibranska I, Hristova E (2011) Comparison of different kinetic models for adsorption of heavy metals onto activated carbon from apricot stones. Bulg Chem Commun 43:370–377
53. Gad HMH, Youssef MA (2018) Sorption behavior of Eu (III) from an aqueous solution onto modified hydroxyapatite: kinetics, modeling and thermodynamics. Environ Technol 39:2583–2596. https://doi.org/10.1080/09593330.2017.1362036
54. Granados-Correa F, Vilchis-Granados J, Jiménez-Reyes M et al (2013) Adsorption behaviour of La(III) and Eu(III) ions from aqueous solutions by hydroxyapatite: kinetic, isotherm, and thermodynamic studies. J Chem 2013:751696. https://doi.org/10.1155/2013/751696
55. Madadrang CJ, Kim HY, Gao G et al (2012) Adsorption behavior of EDTA-Graphene oxide for Pb(II) removal. ACS Appl Mater Interfaces 4:1186–1193. https://doi.org/10.1021/am201645g
56. Akpomie KG, Dawodu FA, Adebowale KO (2015) Mechanism on the sorption of heavy metals from binary-solution by a low cost montmorillonite and its desorption potential. Alex Eng J 54:757–767. https://doi.org/10.1016/j.aej.2015.03.025